35th Annual International Conference of the IEEE EMBS
Osaka, Japan, 3 - 7 July, 2013

Removal of Stimulus-Induced Artifacts in Functional Spinal Cord Imaging

Taishi Watanabe, Yuya Kawabata, Dai Ukegawa, Shigenori Kawabata, Yoshiaki Adachi *Member IEEE*, Kensuke Sekihara, *Fellow IEEE*

***Abstract*— This paper develops a novel method to reduce the influence of stimulus-induced artifacts in functional spinal cord imaging. The developed method employes a two-step procedure. The first step acquires artifact data, which contain artifacts but do not contain spinal cord evoked magnetic field (SCEF). The second step applies a method called common-mode subspace projection (CSP). The effectiveness of the developed method is validated using SCEF data measured from a healthy volunteer.**

I. INTRODUCTION

A nerve conduction block of the cervical spinal cord compressed by intervertebral disks and ligaments may cause numbness and paralysis in the limbs, and such spinal cord disorders are very common[1]. Nonetheless, there are no effective methods for accurate diagnosis of such spinal cord lesions. This is primarily because compression and other spinal cord abnormalities found in patients anatomical images (such as MRI or X-ray images) do not always cause spinal cord disorders.

There have been growing interests in developing biomagnetometers optimized for measuring the spinal cord evoked magnetic field (SCEF)[2][3]. Dynamic (spatio-temporal) source imaging of the spinal cord electrophysiological activity from its evoked magnetic field has also been investigated, aiming at developing a novel, diagnostic imaging tool for cervical spinal cord disorders[4].

One serious problem in implementing such functional spinal cord imaging arises from large stimulus-induced artifacts, which exist from immediately after the stimulus onset to 8–10 ms after it[1]. These artifacts overlap the SCEF signal, and can distort imaging results of spinal cord activity, as shown in our experiments in Section III.

This paper proposes a novel method to reduce the influence of these artifacts in functional spinal cord imaging. The method consists of two steps; the first step acquires the artifact data, the data containing only the artifacts. To obtain such data, we use exactly the same stimulus application procedure to measure SCEF with a stimulus electrode positioned a few centimeters away from the median nerve. The second step applies a method called common-mode subspace projection (CSP), which estimates orthonormal basis of the interference subspace, and projects the measured SCEF data onto the subspace orthogonal to the interference subspace. We validate the method effectiveness using SCEF data measured from a healthy volunteer.

Taishi Watanabe, Yoya Kawabata, and Kensuke Sekihara are with the Department of Systems Design and Engineering, Tokyo Metropolitan University, Asahigaoka 6-6, Hino, Tokyo 191-0065, Japan.

Dai Ukegawa, and Shigenori Kawabata are with the Department of Orthopedic Surgery, Tokyo Medical and Dental University, Tokyo 113-859, Japan.

Yoshiaki Adachi is with the Applied Electronics Laboratory, Kanazawa Institute of Technology, Kanazawa, 921-1331, Japan.

Kensuke Sekihara is a corresponding author(e-mail: ksekiha@sd.tmu.ac.jp)

[1]Although exact causes of these artifacts are unexplored, we speculate that they are caused by combined effects of body electric currents induced by the stimulus and transient responses of receiver electronics.

II. METHOD

A. Data Model and Signal-Space Projection

Defining the spatio-temporal data matrix as $\boldsymbol{B}$ in which the (i, j) element is the output of the ith sensor at the jth time point. Let us define the number of sensors and the number of time points as M and T, respectively. The $M \times T$ spatio-temporal data matrix $\boldsymbol{B}$ is expressed as

$$\boldsymbol{B} = \boldsymbol{B}_S + \boldsymbol{B}_I, \tag{1}$$

where $\boldsymbol{B}_S$ is the SCEF signal, and $\boldsymbol{B}_I$ is the interference referred to as the artifacts. We can obtain a separate "control" measurement $\boldsymbol{A}$ that contains only $\boldsymbol{B}_I$. Such data is referred to as the artifact measurement in this paper, and expressed ideally as

$$\boldsymbol{A} = \boldsymbol{B}_I. \tag{2}$$

A well-known method to reduce the artifacts under the model expressed in Eqs. (1) and (2) is a method called signal-space projection (SSP)[5][6]. This method uses the orthonormal basis of the interference subspace, which can be estimated by applying the singular-value decomposition (SVD) to the spatio-temporal matrix $\boldsymbol{A}$. Applying SVD, we have

$$\boldsymbol{A} = [\boldsymbol{f}_1, \ldots, \boldsymbol{f}_M] \begin{bmatrix} \gamma_1 & 0 & \cdots & 0 \\ 0 & \gamma_2 & \cdots & 0 \\ \vdots & \vdots & \ddots & \vdots \\ 0 & 0 & \ldots & \gamma_M \end{bmatrix} \begin{bmatrix} \boldsymbol{g}_1^T \\ \vdots \\ \boldsymbol{g}_M^T \end{bmatrix}, \tag{3}$$

where we assume $M \leq T$ If the singular values $\gamma_1, \gamma_2, \ldots, \gamma_p$ are distinctively large, spatial singular vectors $\boldsymbol{f}_1, \ldots, \boldsymbol{f}_p$ can be considered the orthonormal basis of the interference subspace, i.e., these singular vectors span the interference subspace. Thus, defining $\boldsymbol{F}_p = \big[\boldsymbol{f}_1, \ldots, \boldsymbol{f}_p\big]$, the matrix $\boldsymbol{I} - \boldsymbol{F}_p \boldsymbol{F}_p^T$ projects a data vector onto the subspace that is orthogonal to the interference subspace, and the artifacts can be removed by using $(\boldsymbol{I} - \boldsymbol{F}_p \boldsymbol{F}_p^T)\boldsymbol{B}$.

978-1-4577-0216-7/13/$26.00 ©2013 IEEE

However, when the artifact measurement $\boldsymbol{A}$ contains additional components that do not exist in the SCEF measurement $\boldsymbol{B}$, SSP may cause erroneous results. We next describe common-mode subspace projection (CSP), which is considered effective even in such situations. The basic idea of CSP was reported in [7].

B. Common-Mode Subspace Projection (CSP)

In the CSP method, we assume that the artifact measurement $\boldsymbol{A}$ actually contains an additional component $\boldsymbol{B}_A$, such that

$$\boldsymbol{A} = \boldsymbol{B}_I + \boldsymbol{B}_A. \tag{4}$$

The measured data $\boldsymbol{B}$ are expressed in Eq. (1). Therefore, the interference is a common component between $\boldsymbol{A}$ and $\boldsymbol{B}$, i.e., the interference subspace is the intersection of the subspaces of the SCEF measurement and of artifact measurement.

Let us define the subspace of the SCEF measurement as $\mathcal{S}_B$ and that of the artifact measurement as $\mathcal{S}_A$. To obtain the orthonormal basis of $\mathcal{S}_B$, we apply SVD to $\boldsymbol{B}$, such that

$$\boldsymbol{B} = [\boldsymbol{d}_1, \ldots, \boldsymbol{d}_M] \begin{bmatrix} \lambda_1 & 0 & \cdots & 0 \\ 0 & \lambda_2 & \cdots & 0 \\ \vdots & \vdots & \ddots & \vdots \\ 0 & 0 & \ldots & \lambda_M \end{bmatrix} \begin{bmatrix} \boldsymbol{e}_1^T \\ \vdots \\ \boldsymbol{e}_M^T \end{bmatrix}, \tag{5}$$

where $\boldsymbol{d}_1, \ldots, \boldsymbol{d}_M$ and $\boldsymbol{e}_1, \ldots, \boldsymbol{e}_M$ are the spatial and temporal singular vectors, and $\lambda_1, \ldots, \lambda_M$ are the singular values of $\boldsymbol{B}$. In this paper, we are interested in the subspace spanned by temporal vectors. Thus, the orthonormal temporal basis set of $\mathcal{S}_B$ is $\{\boldsymbol{e}_1, \ldots, \boldsymbol{e}_q\}$ where q is the number of distinctively large singular values. According to Eq. (3), the orthonormal temporal basis set of $\mathcal{S}_A$ is $\{\boldsymbol{g}_1, \ldots, \boldsymbol{g}_p\}$ where p is the number of distinctively large singular values. The interference subspace is the intersection of $\mathcal{S}_A$ and $\mathcal{S}_B$, i.e., $\mathcal{S}_A \cap \mathcal{S}_B$.

The procedure to find the intersection according to [8] is described below. The orthonormal basis set of the intersection is expressed as a set of the principal vectors between $\mathcal{S}_A$ and $\mathcal{S}_B$ whose principal angle is equal to zero. To find those principal vectors, we first define

$$\boldsymbol{E}_q = [\boldsymbol{e}_1, \ldots, \boldsymbol{e}_q], \tag{6}$$

$$\boldsymbol{G}_p = [\boldsymbol{g}_1, \ldots, \boldsymbol{g}_p]. \tag{7}$$

The singular-value decomposition of a matrix $\boldsymbol{E}_q^T \boldsymbol{G}_p$ is performed, such that

$$\boldsymbol{Y}^T \left(\boldsymbol{E}_q^T \boldsymbol{G}_p \right) \boldsymbol{Z} = \begin{bmatrix} \cos(\theta_1) & \cdots & 0 \\ \vdots & \ddots & \vdots \\ 0 & \ldots & \cos(\theta_q) \end{bmatrix}, \tag{8}$$

where the singular values are equal to the cosine of the principal angles between $\mathcal{S}_A$ and $\mathcal{S}_B$. The intersection $\mathcal{S}_A \cap \mathcal{S}_B$ has a property that the principal angles are equal to zero. Thus, by finding the relationship,

$$\cos(\theta_1) = \cos(\theta_2) = \cdots = \cos(\theta_r) \approx 1,$$

the dimension of $\mathcal{S}_A \cap \mathcal{S}_B$ is determined to be r.

The principal vectors are then obtained either as the first r columns of a matrix $\boldsymbol{E}_q \boldsymbol{Y}$ or the first r columns of a matrix $\boldsymbol{G}_p \boldsymbol{Z}$. Let us define the first r columns of $\boldsymbol{E}_q \boldsymbol{Y}$ as $\boldsymbol{u}_1, \ldots, \boldsymbol{u}_r$, and a matrix $\boldsymbol{U}_r$ as $\boldsymbol{U}_r = [\boldsymbol{u}_1, \ldots, \boldsymbol{u}_r]$. Since the vectors $\boldsymbol{u}_1, \ldots, \boldsymbol{u}_r$ are orthonormal basis of $\mathcal{S}_A \cap \mathcal{S}_B$, which is the interference subspace, the artifact removal is carried out by right multiplying $(\boldsymbol{I} - \boldsymbol{U}_r \boldsymbol{U}_r^T)$ to the measured data $\boldsymbol{B}$, i.e., by using $\boldsymbol{B}(\boldsymbol{I} - \boldsymbol{U}_r \boldsymbol{U}_r^T)$.

III. EXPERIMENTS

A. SCEF and Artifact Measurements

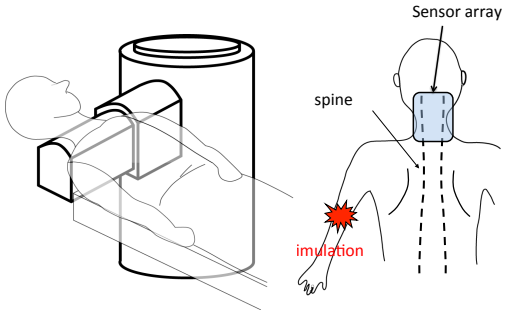

Fig. 1. Schematic illustration of measurement setup. The subject lies down in the supine position, and the subjects lower neck is positioned on the upper surface of the protrusion of the cryostat. A stimulus current was applied to the subject's median nerve near the elbow

A recently-developed 120-channel biomagnetometer [3][9] was used for measuring the human SCEF. The experimental setup is schematically shown in Fig. 1. As depicted in this figure, the cryostat of the biomagnetometer has a cylindrical body with a protrusion, and this protrusion part contains sensors in the upward direction. The biomagnetometer is equipped with 40 vector sensors, which are arranged at 8×5 measurement locations covering an 14×9 cm area. The subject lies down in the supine position, and the subjects lower neck is positioned on the upper surface of the protrusion of the cryostat.

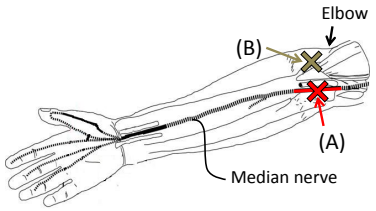

Fig. 2. Schematic illustration of locations for stimulus applications. The location (A) is for measuring SCEF, and the location (B) is for acquiring the artifact measurement.

The subject was a healthy male volunteer. The experiment was approved by an ethics committee of Tokyo Medical and

Dental University. A stimulus current was applied to the subjects median nerve near his elbow. The stimulus with intensity of 10 mA and 0.3 ms duration was repeated 2000 times at a repetition rate of 4 Hz. The data acquisition was performed with sampling frequency of 40 kHz. An analog bandpass filter with a bandwidth of 100-5000 Hz was applied. The signal was averaged across all 2000 measured trials.

To obtain the artifact data, we applied exactly the same stimulus with a stimulus electrode positioned a few centimeters away from the median nerve. The locations for stimulus application are schematically shown in Fig. 2. In this figure, the location labeled by (A) is the stimulus electrode location for measuring SCEF, which is on the medium nerve near subject's elbow. The location labeled by (B) is the stimulus electrode location for acquiring the artifact data. The location is approximately 2 cm away from the medium nerve. Therefore, even applying the same stimulus, it did not elicit the nerve activity. Since the stimulus condition is exactly the same, artifacts similar to those contained in the measured SCEF data can be induced.

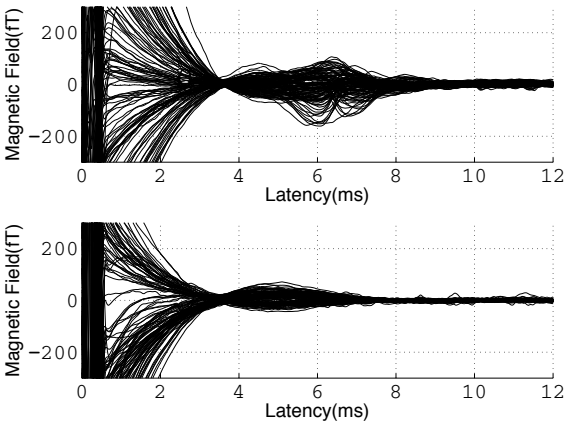

Fig. 3. The measured SCEF (top) and artifact data (bottom). The origin of the latency is the onset of the stimulus.

The measured SCEF, after averaging 2000 trials, is shown in the top panel of Fig. 3. The electric stimulus was given at the latency of 0 ms. The SCEF signal is observed in the time window between 4 and 8 ms. However, large artifacts are observed before 4 ms. The artifact measurement is shown in the bottom panel of Fig. 3. We can see that artifacts very similar to those in the SCEF data (top panel) exist in the bottom plots. Also, the artifact time courses in the bottom panel show a dull peak around 4–8 ms. Thus, the SCEF data in the top panel should contain artifacts even after 4 ms.

B. Artifact Removal

We applied CSP described in Section II to the SCEF data in Fig. 3. Before applying CSP, we applied a preprocessing procedure called the power correction, which made the power of the artifact measurement to be equal to that of the SCEF data. This correction was performed in a sensor-channel by sensor-channel manner. That is, defining the weight vector $\boldsymbol{w} = [w_1, \ldots, w_M]$, we created the power corrected artifact measurement $\widetilde{A}$ through $\widetilde{A} = \boldsymbol{w}^T \boldsymbol{A}$. The weight for the ith sensor channel w_i was obtained using

$$w_i = \arg\min_{w} \sum_{j} \left(B_{i,j} - wA_{i,j}\right)^2 .$$

The CSP method used the SCEF data $\boldsymbol{B}$ and the power-corrected data $\widetilde{A}$ to extract orthonormal basis vectors of the (common) interference subspace. Then, it projected the data $\boldsymbol{B}$ onto the subspace orthogonal to the interference subspace. The results of this artifact removal are shown in the bottom panel of Fig. 4. In the top panel of Fig. 4, the same SCEF data as shown in the top panel of Fig. 3 are again shown for comparison. Note that the scale in the ordinate is different between Figs. 3 and 4.

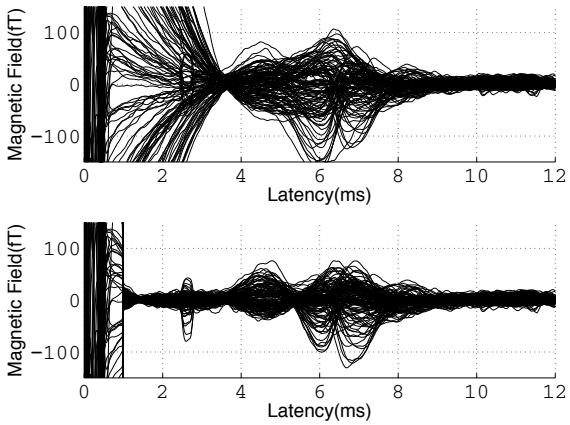

Fig. 4. The measured SCEF (top) and artifact-removed results (bottom). The measured SCEF in the top panel is the same as that in the top panel in Fig. 3 with different scale in the ordinate. The sharp peak between 2 and 3 ms in artifact-removed results appeared due to some hardware problems, so it should be disregarded.

The results in the bottom plots of Fig. 4 indicate that the artifacts are significantly reduced and the peaks due to spinal cord activity between 4 and 8 ms are more clearly be observed, indicating the effectiveness of the proposed method.

C. Validation in Source Space

We then proceeded with source imaging, and validated the effectiveness of the proposed artifact removal method in the source space. To perform source reconstruction, an X-ray image covering the subject's neck and sensors was obtained for identifying the location of the spinal cord, and a curved plane containing the spinal cord was determined as the reconstructed region (source space). Such an X-ray image with the extracted 2-D source space is shown in Fig. 5.

The spinal cord source activity was reconstructed on this plane using the recursively-updated null-steering (RENS) beamformer described in [10]. The relative position of reconstruction region to the subject neck and the coordinate system are shown in Fig. 6. The reconstruction area, indicated by the square in Fig. 6, consists of 16×12.5 cm. The voxel interval is 0.5 cm in the x and y directions. The reconstructed

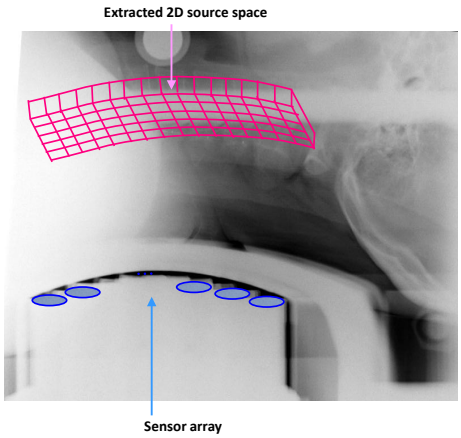

Fig. 5. X-ray image covering the subject neck and the sensors used for extracting a curved plane containing the spinal cord. The extracted plane and sensors are shown.

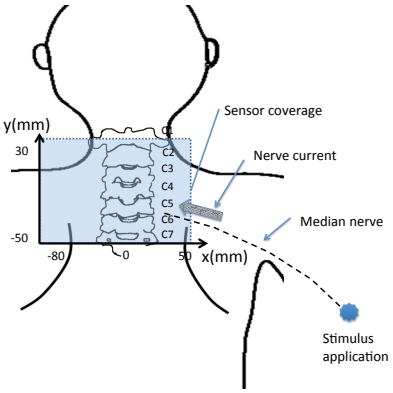

Fig. 6. Schematic illustration of the reconstruction region. Relative positions to subject's neck and the median nerve are shown.

source images at the latency of 5.8 ms are shown in Fig. 7. In this figure, the source image from the original SCEF data are shown in (a). The image from the artifact-removed SCEF data are shown in (b). Both results show the leading dipole (intercellular current) but the direction of the leading dipole (indicated by the white arrow) is significantly different between these two images.

To determine which results are physiologically more plausible, we use the source image obtained with the stimulus applied at the median nerve near subject's wrist (Fig. 7(c)). The SCEF signal obtained with the wrist stimulation is significantly less affected by the artifacts. Taking a look at the direction of the leading dipole, the direction has the transverse (the negative x) component in (b) and (c), while the current direction is almost upward in (a), i.e., the current vector had almost no x component.

Since the subject's left median nerve was stimulated, the nerve activity propagated from the left median nerve into the spinal cord in a region below the fourth vertebra (c4), and thus, it should be more plausible that the current vector had a transverse, negative x component, as depicted in Fig. 6.

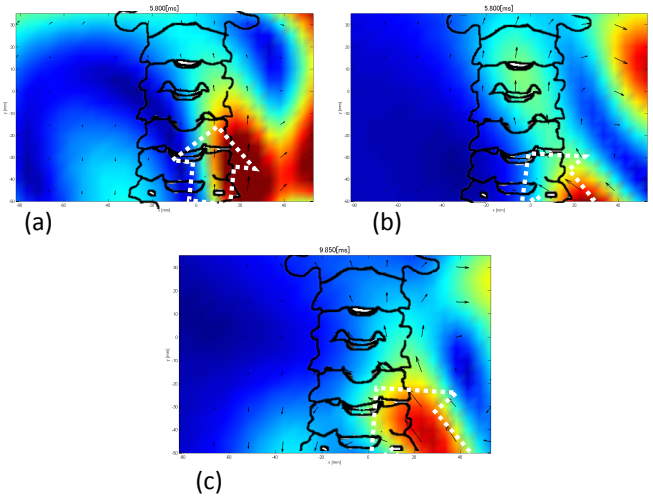

Fig. 7. (a) Source image at the latency of 5.8 ms obtained from the original SCEF data. (b) Source image at the latency of 5.8 ms from the artifact-removed SCEF data. (c) Source image at 9.85 ms obtained from the original SCEF data obtained with the stimulus applied at the median nerve near subject's wrist. The white arrows indicate the direction of the leading dipole (intercellular current). Reconstruction was performed using the recursively-updated null-steering (RENS) beamformer in [10].

Accordingly, the results in (b) are physiologically more plausible than those in (a), indicating the effectiveness of the proposed method.

REFERENCES

[1] K. Shinomiya, K. Furuya, R. Sato, A. Okamoto, Y. Kurosa, and M. Fuchioka, "Electrophysiologic diagnosis of cervical OPLL myelopathy using evoked spinal cord potentials," *Spine*, vol. 13, pp. 1225–1233, 1998.

[2] S. Kawabata, H. Komori, K. Mochida, H. Ohkubo, and K. Shinomiya, "Visualization of conductive spinal cord activity using a biomagnetometer," *Spine*, vol. 27, pp. 475–479, 2003.

[3] Y. Adachi, J. Kawai, M. Miyamoto, H. Ogata, M. Tomori, S. Kawabata, T. Sato, and G. Uehara, "A squid system for measurement of spinal cord evoked field of supine subjects," *IEEE Trans. Appl. Supercond.*, vol. 19, pp. 861–866, 2009.

[4] T. Sato, Y. Adachi, M. Tomori, S. Ishii, S. Kawabata, and K. Sekihara, "Functional imaging of spinal cord electrical activity from its evoked magnetic field.," *IEEE Trans. Biomed. Eng.*, vol. 56, pp. 2452–60, 2009.

[5] M. Huotilainen, R. J. Ilmoniemi, H. Tiitinen, J. Lavikainen, K. Alho, M. Kajola, J. Simola, and R. Naäätaäen, "Eye-blink removal for multichannel MEG measurements," in *Abstract Book for 8th International Conference on Biomagnetism* (L. Deecke *et al.*, eds.), (Vienna, Austria), pp. 209–210, 1993.

[6] G. Nolte and G. Curio, "The effect of signal-space projection on dipole localization accuracy," *IEEE Trans. Biomed. Eng.*, vol. 46, pp. 400–408, 1999.

[7] S. Taulu and J. Simola, "Spatiotemporal signal space separation method for rejecting nearby interference in MEG measurements," *Phys. Med. Biol.*, vol. 51, pp. 1759–68, 2006.

[8] G. H. Golub and C. F. V. Loan, *Matrix computations: third edition*. Baltimore and London: The Johns Hopkins University Press, 1996.

[9] Y. Adachi, J. Kawai, M. Miyamoto, H. Ogata, M. Tomori, S. Kawabata, T. Sato, and G. Uehara, "Improvement of squid magnetometer system for extending application of spinal cord evoked magnetic field measurement," *IEEE Trans. Appl. Supercond.*, vol. 21, pp. 485–488, 2011.

[10] I. Kumihashi and K. Sekihara, "Array-gain constraint minimum-norm spatial filter with recursively updated gram matrix for biomagnetic source imaging.," *IEEE Trans. Biomed. Eng.*, vol. 57, pp. 1358–65, 2010.